Electronic Supplementary Material (ESI) for Dalton Transactions.

Electronic Supplementary Information (ESI)

Aggregation-Induced Emission (AIE) active probe for multiple targets: Fluorescent sensor for Zn^{2+} and Al^{3+} & colorimetric sensor for Cu^{2+} and F^{-}

Soham Samanta, Utsab Manna, Turjya Ray and Gopal Das *

Department of Chemistry
Indian Institute of Technology Guwahati, Guwahati 781039, Assam, India
E-mail: gdas@iitg.ernet.in

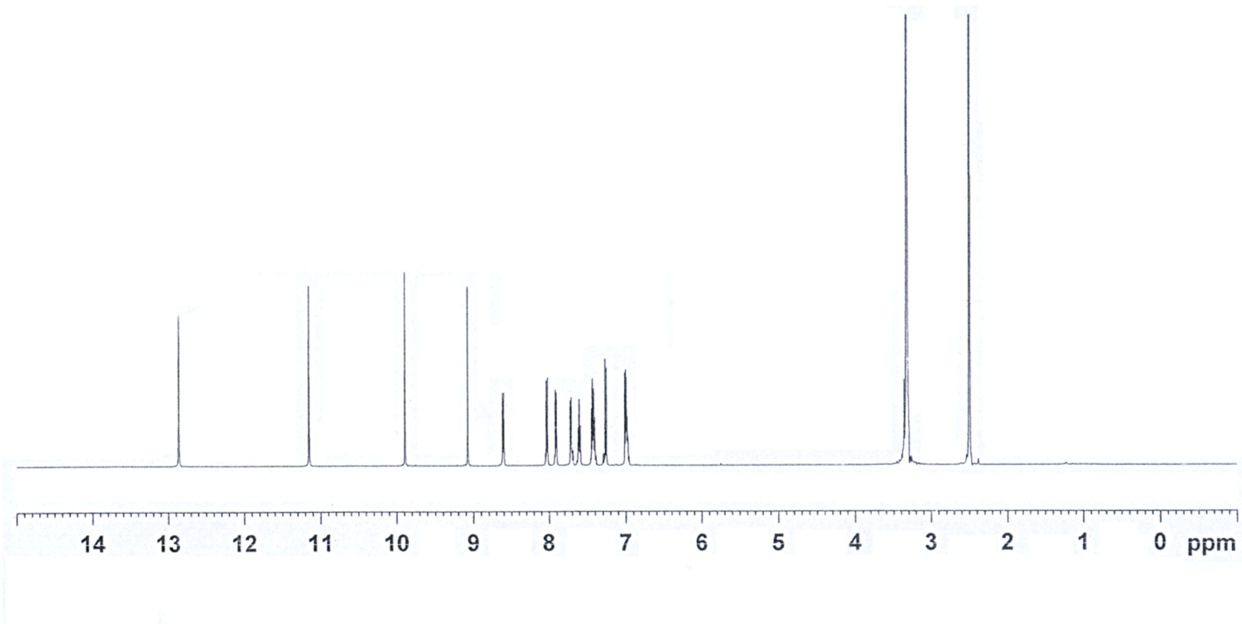

Figure S1. ^{1}H-NMR spectra of **L**.

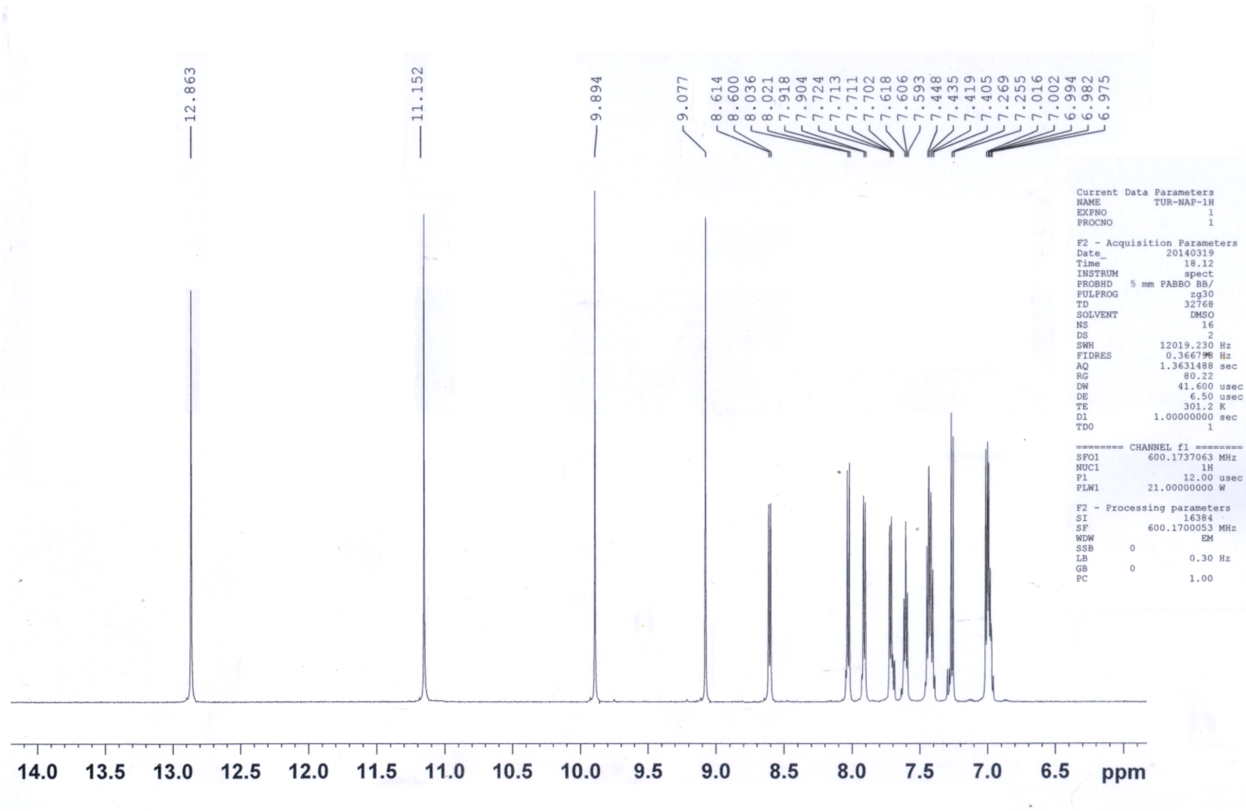

Figure S2. Expanded ^{1}H-NMR spectra of **L**.

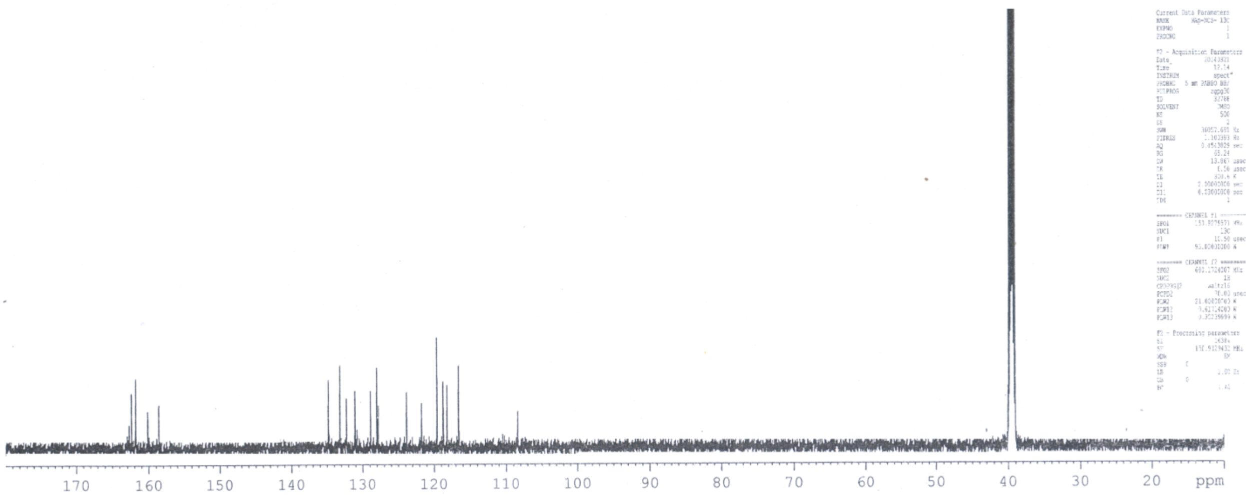

Figure S3. ^{13}C-NMR spectra of **L**.

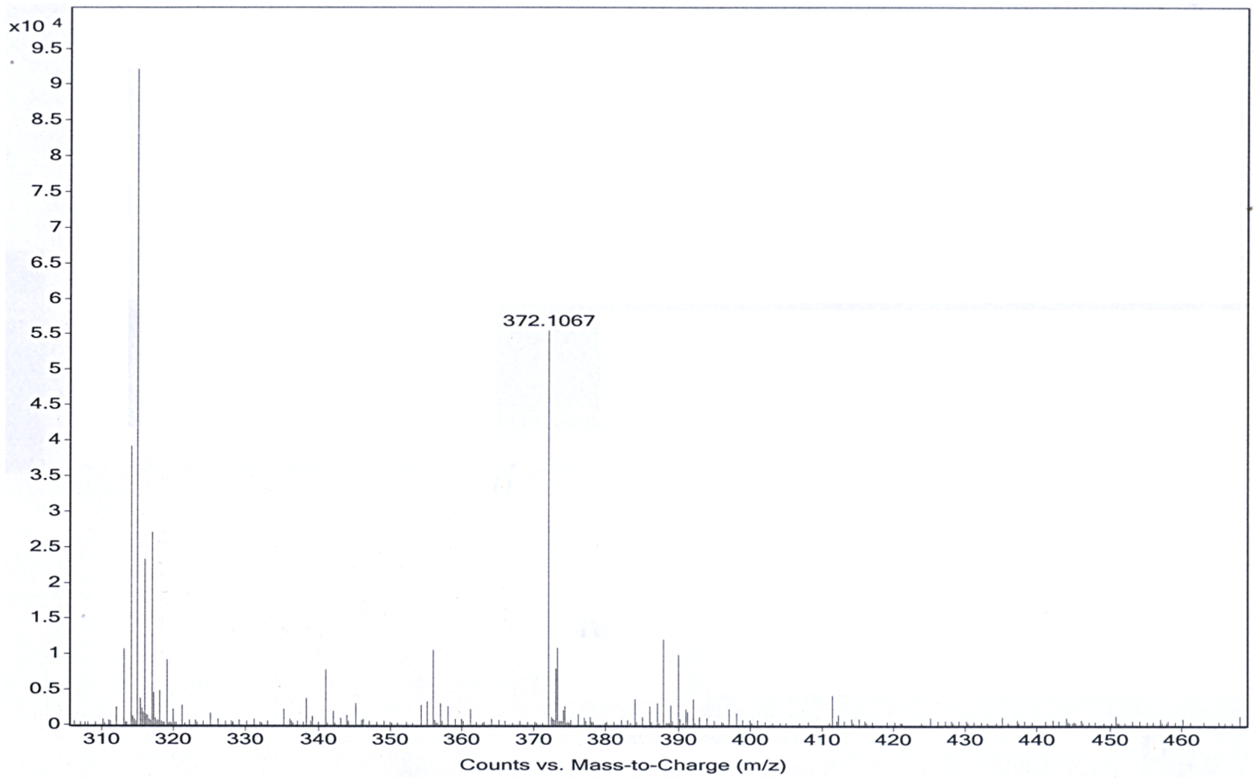

Figure S4. Mass spectrum of **L**.

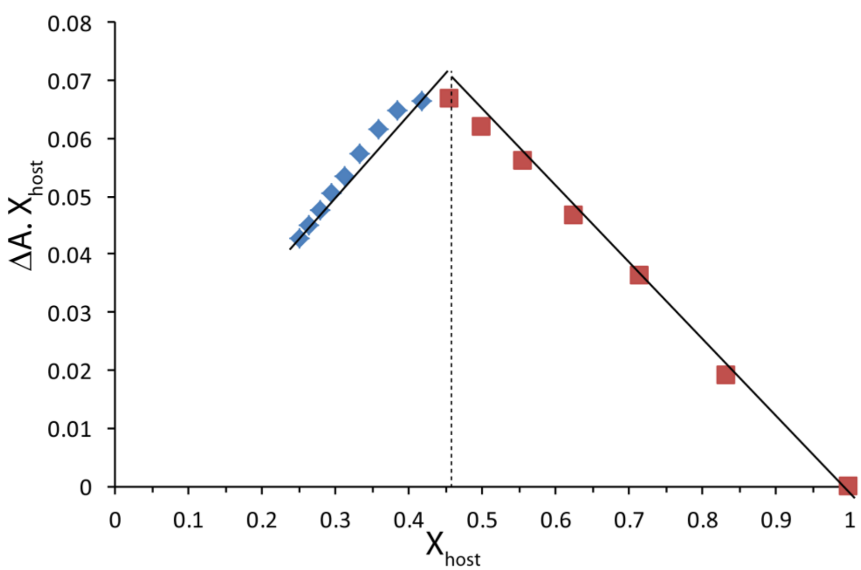

Figure S5: Job's plot for Cu^{2+} from the titration spectra.

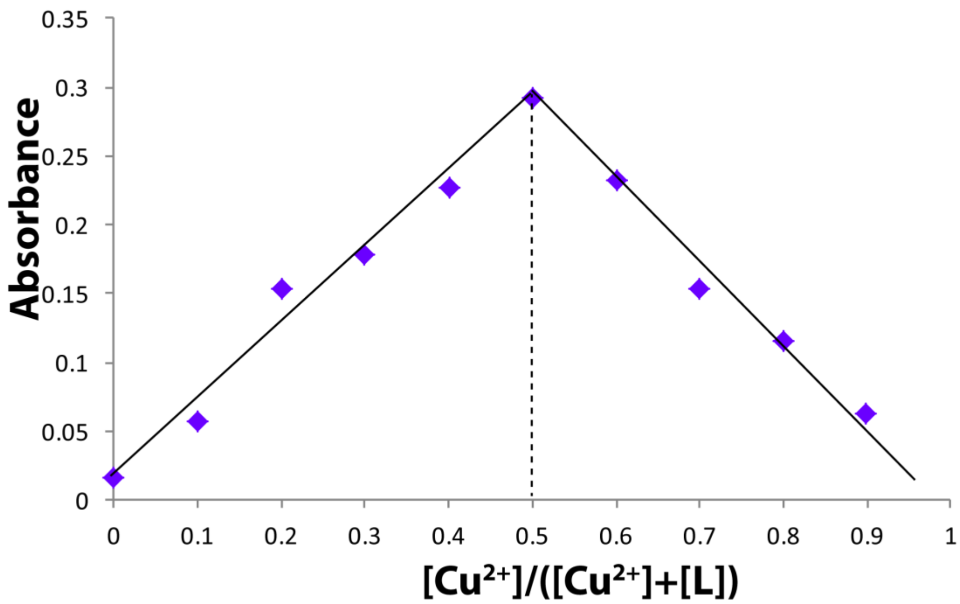

Figure S6: Job's plot for Cu^{2+} indicating 1:1 chelation from conventional Job's plot experiment.

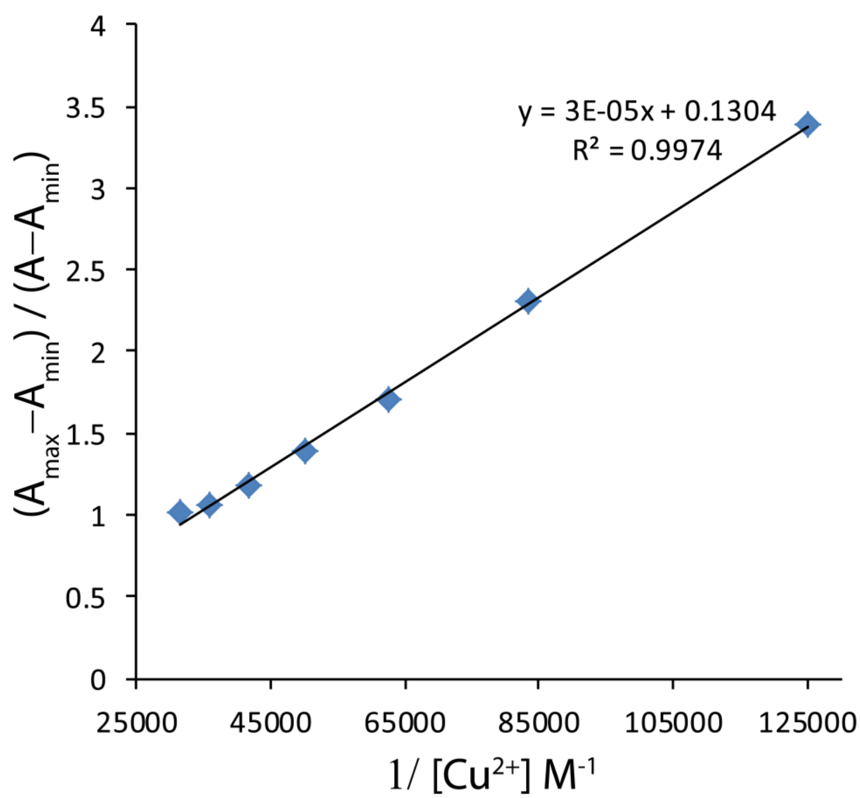

Figure S7. : B-H plot for determination of Binding constant for Cu^{2+}.

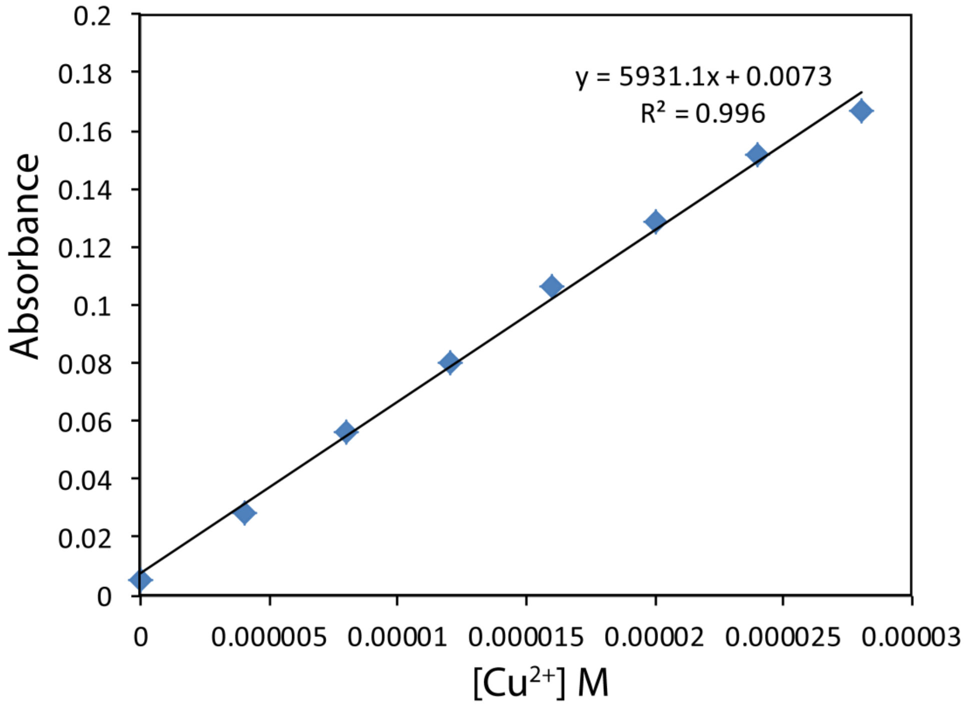

Figure S8. Absorbance vs. concentration of Cu^{2+} plot for determination of detection limit.

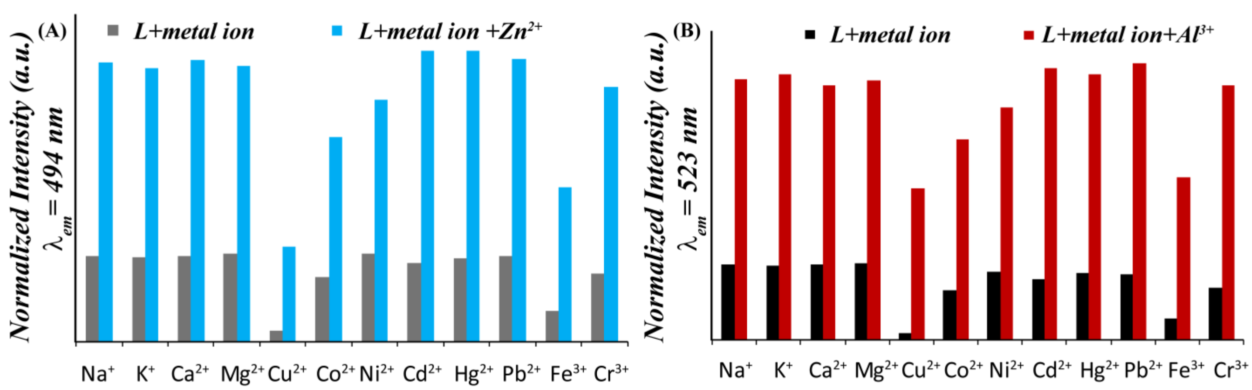

Figure S9. (A) Interference of other metal ions in Zn^{2+} sensing. In the solution of **L** (10μM) various metal ions (100μM) were added followed by addition of Zn^{2+} (100μM) in 9:1 methanol/HEPES buffer (5mM, pH 7.3; 9:1, v/v) medium. (B) Interference of other metal ions in Al^{3+} sensing. In the solution of **L** (10μM) various metal ions (100μM) were added followed by addition of Al^{3+} (100μM) in 9:1 methanol/HEPES buffer (5mM, pH 7.3; 9:1, v/v) medium.

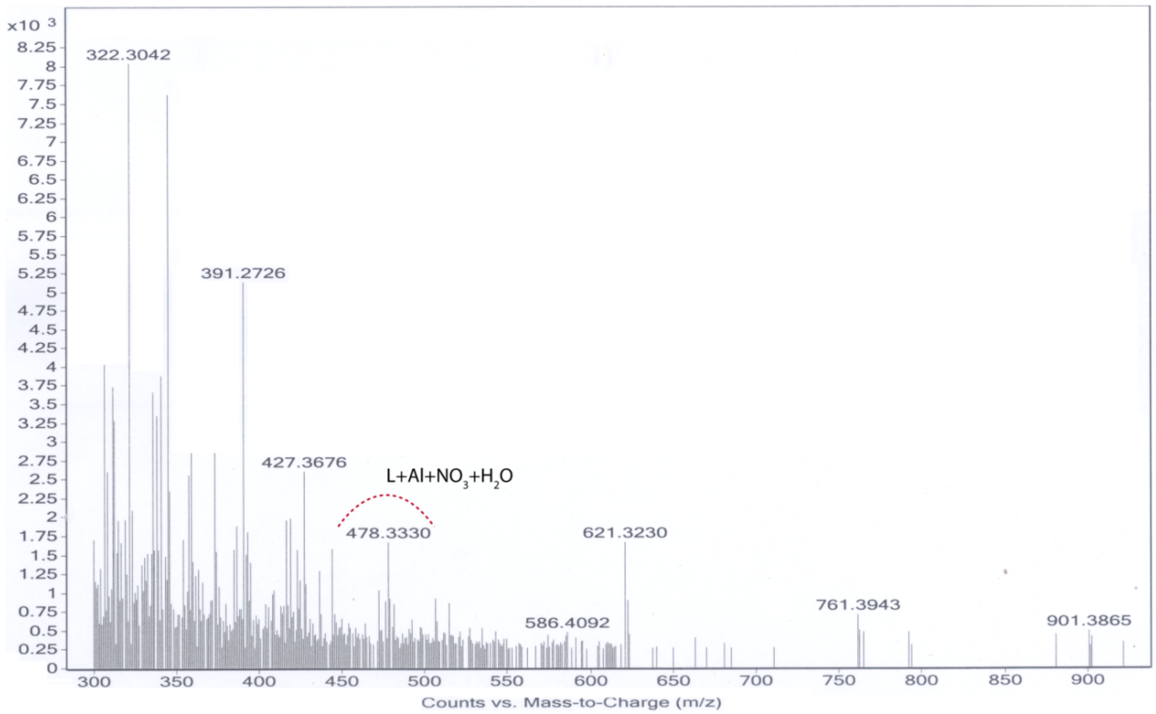

Figure S10. Mass spectrum of L in presence of Al^{3+}

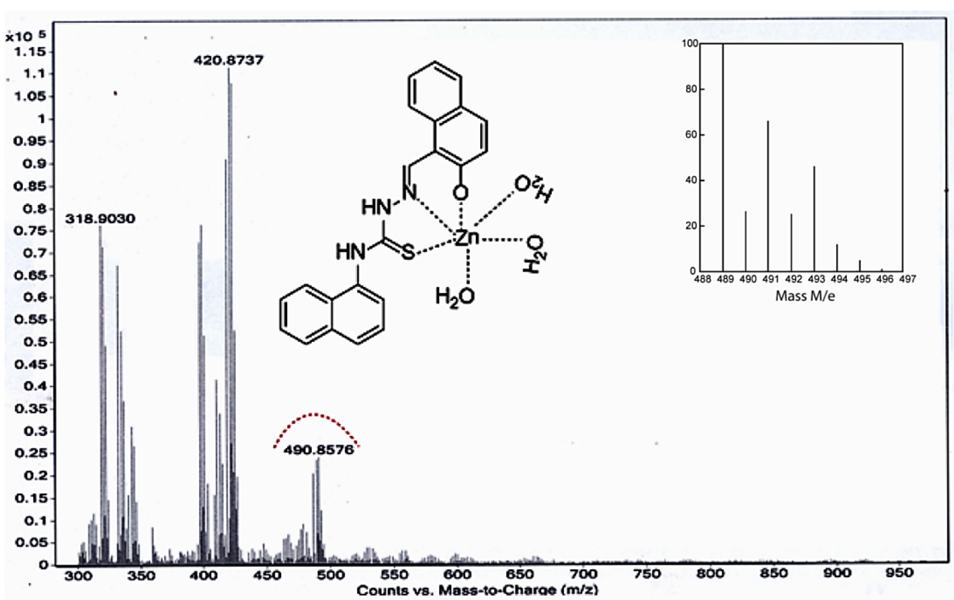

Figure S11. Mass spectrum of **L** in presence of Zn^{2+}; as expected the isotope pattern of Zn-complex is matched well with the observed mass spectra with peaks separated by m/z 2.

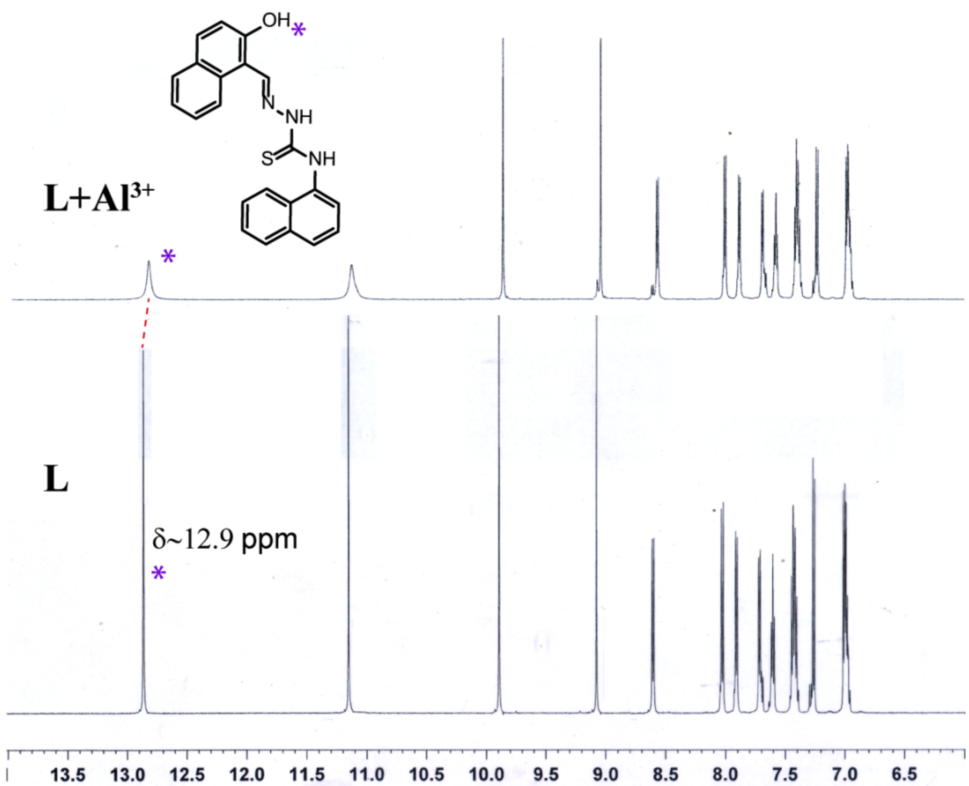

Figure S12. ^{1}H NMR spectrum of **L** in presence of Al^{3+} in DMSO-d_6

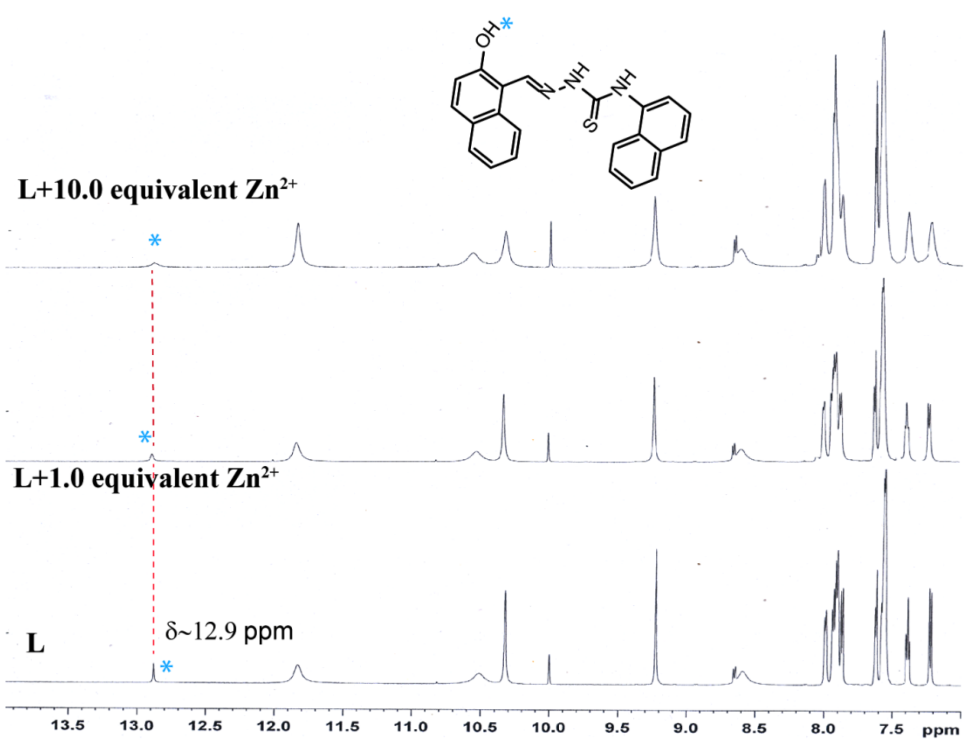

Figure S13. ^{1}H NMR spectrum of L in presence of Zn^{2+} in DMSO-d_6

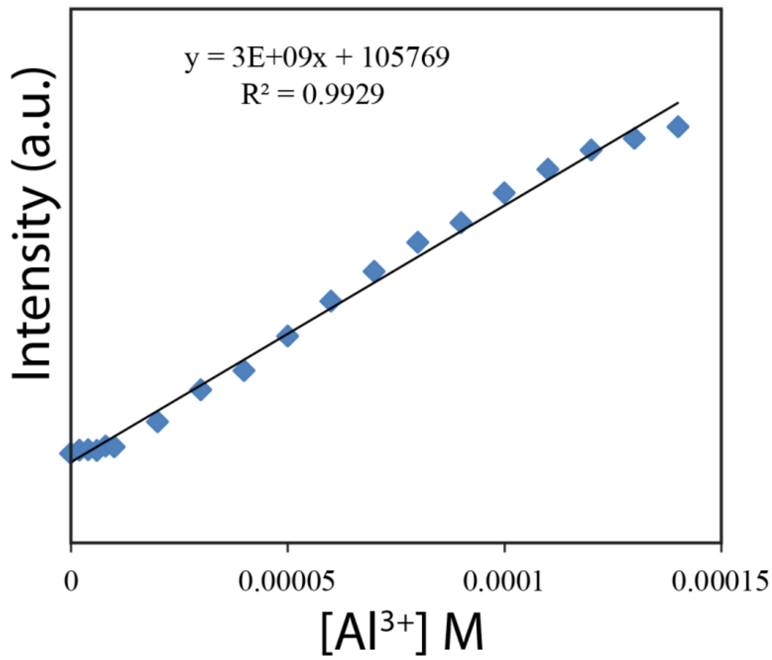

Figure S14. Fluorescence intensity vs. concentration of Al^{3+} plot for determination of detection limit

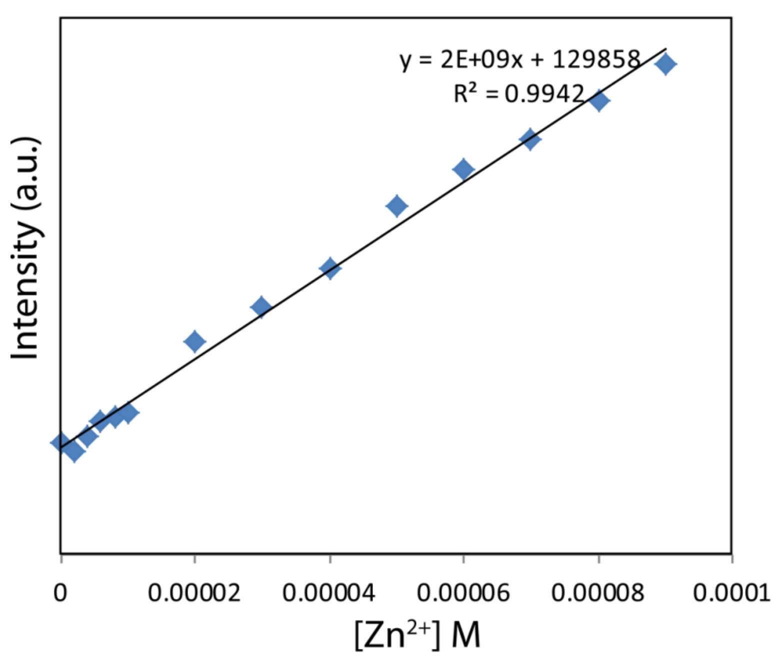

Figure S15. Fluorescence intensity vs. concentration of Zn^{2+} plot for determination of detection limit

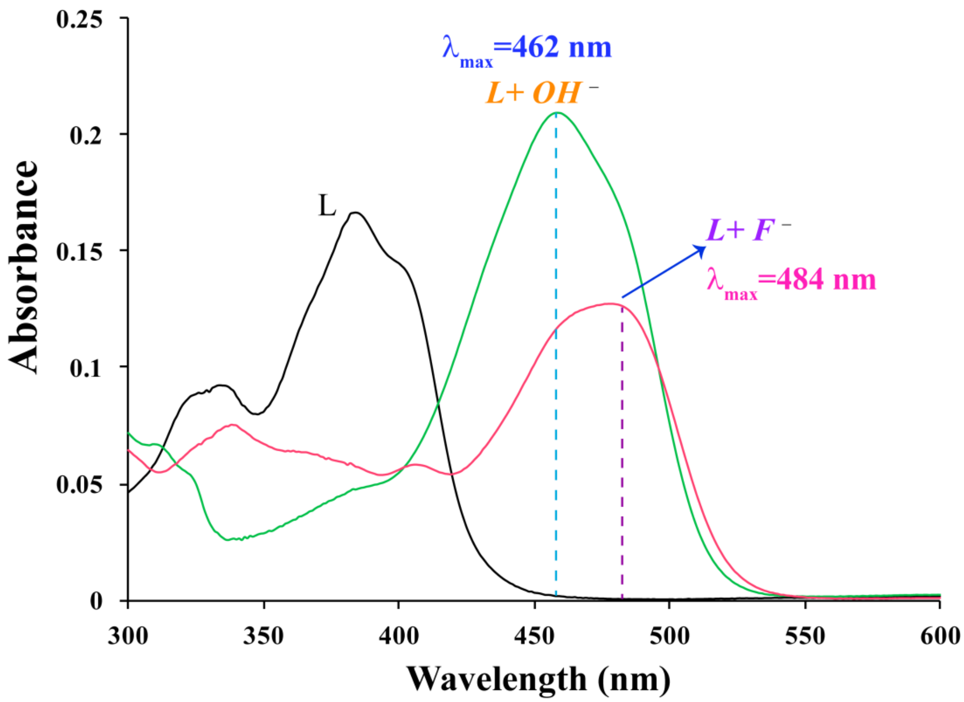

Figure S16: UV-Vis spectra of L (5mM) in presence of 10 equivalents of tetra-butyl ammonium hydroxide and tetra-butyl ammonium fluoride in acetonitrile

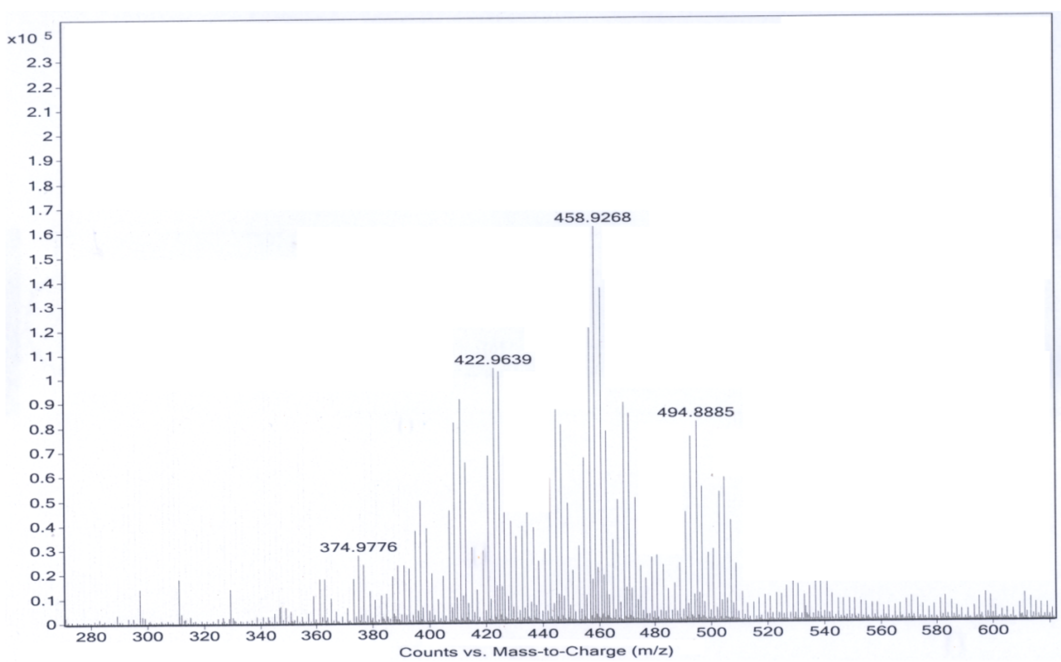

Figure S17. Mass spectrum of **L** in presence of Fluoride

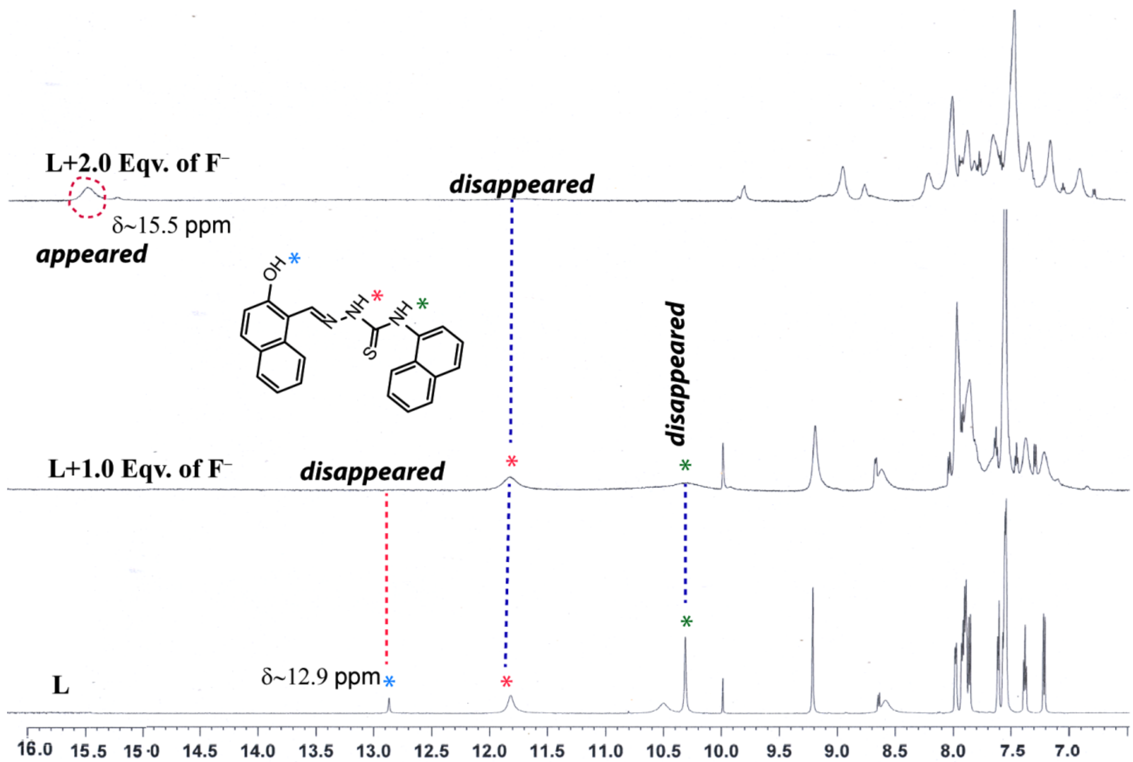

Figure S18. ^{1}H NMR spectrum of L in presence of tetra-butyl ammonium fluoride in DMSO-d_6

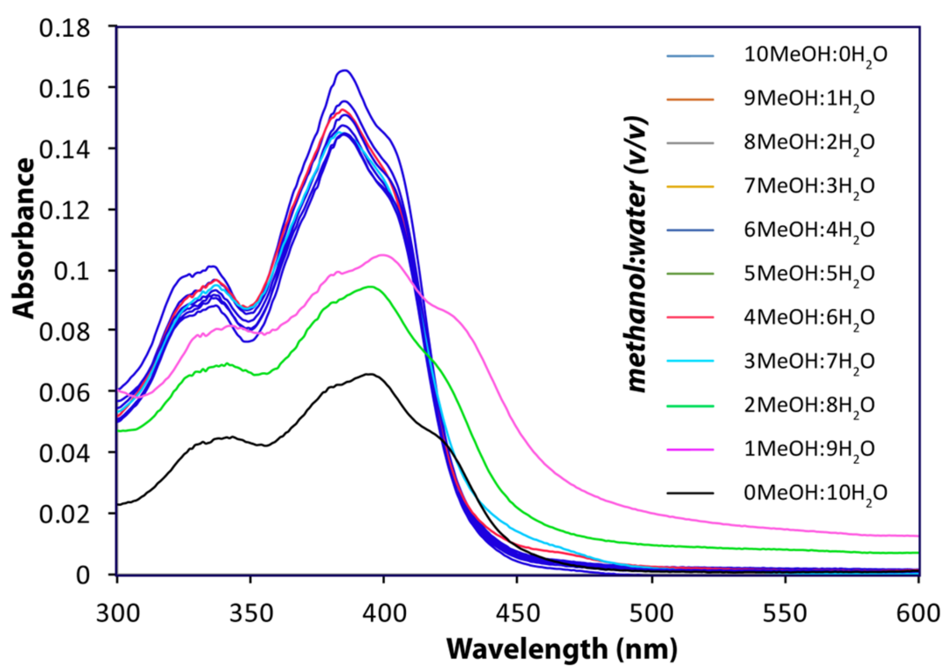

Figure S19. UV-Vis spectra of L (5μM) in methanol-water medium with different water fraction

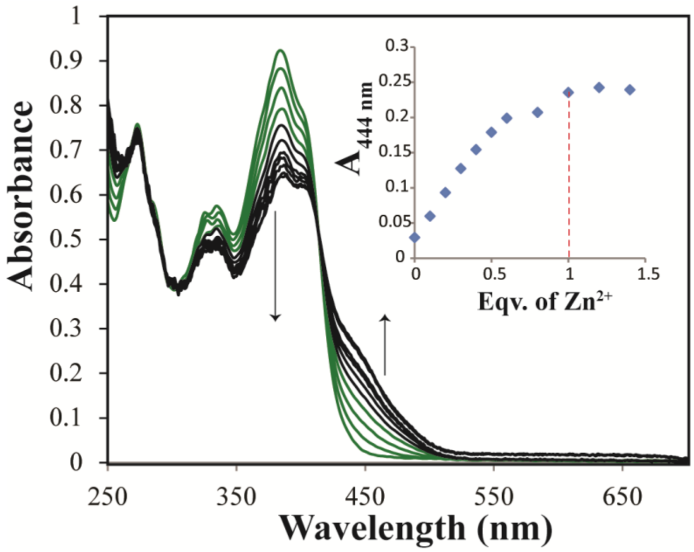

Figure S20. Figure S20. UV-Vis spectra of **L** (25µM) with gradual incremental addition of Zn^{2+} in methanol; Inset: change in absorbance at 444 nm with added equivalent of Zn^{2+}. With gradual incremental addition of Zn^{2+} to **L** in methanol medium exhibited slight growth in absorbance at 444 nm with subsequent downfall of the absorbance at 384 nm to generate a well-defined isosbestic point at around 420 nm. The titration curve shows a saturation after addition of 1 equivalent of Zn^{2+} which hints towards 1:1 chelation between **L**-Zn^{2+}.

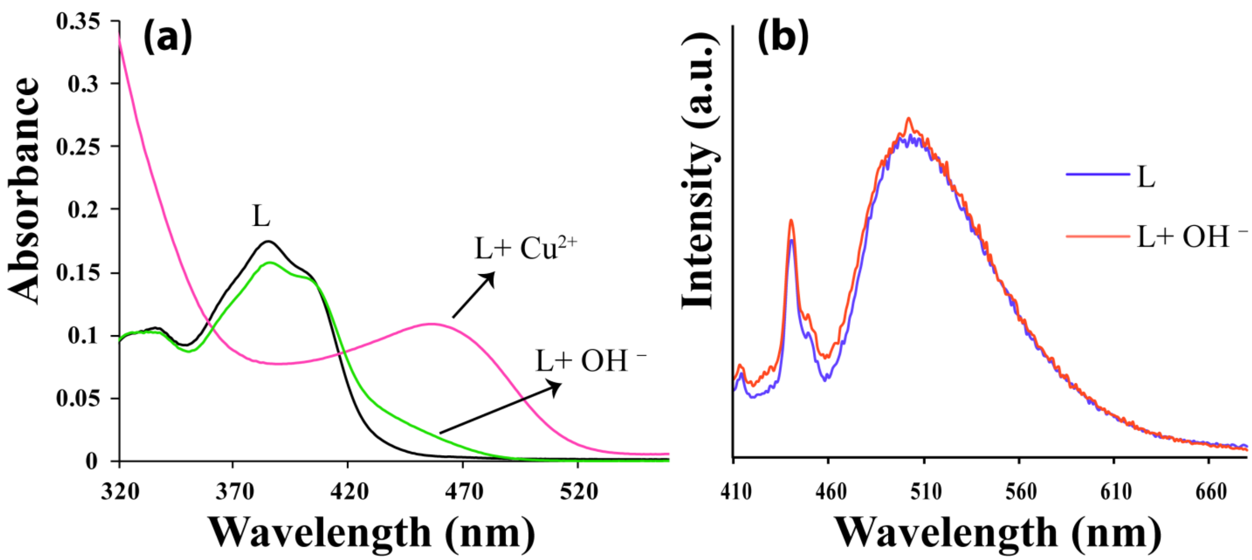

Figure S21. (a) UV-Vis spectra of **L** (5µM) in presence of Cu^{2+} (50µM) and hydroxide (50µM) in CH_3OH/aqueous HEPES buffer (5 mM, pH 7.3; 9:1, v/v) medium. (b) Fluorescence spectra of **L** (5µM) in presence of hydroxide in CH_3OH/aqueous HEPES buffer (5 mM, pH 7.3; 9:1, v/v) medium; λ_{ex}=390 nm.

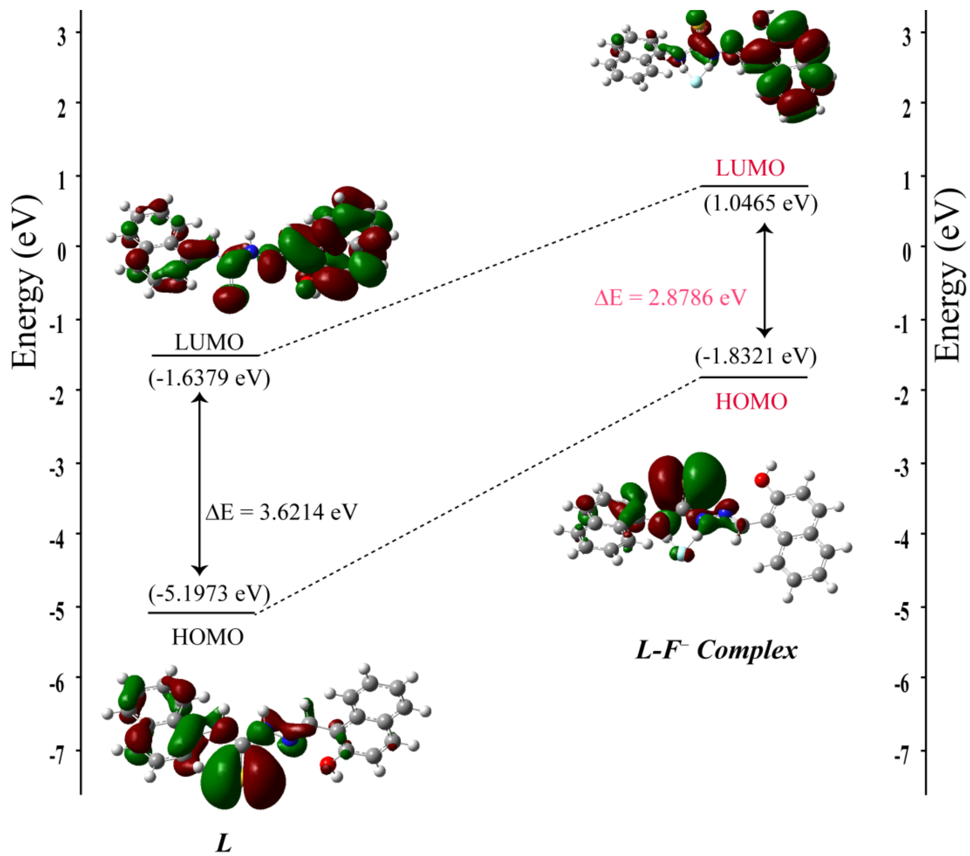

Figure S22: Frontier molecular orbital plots and energy level diagrams of **L** and **L**-F^{-} complex. The calculations were performed using B3LYP/6-31 G (d,p) as implemented on Gaussian 03.

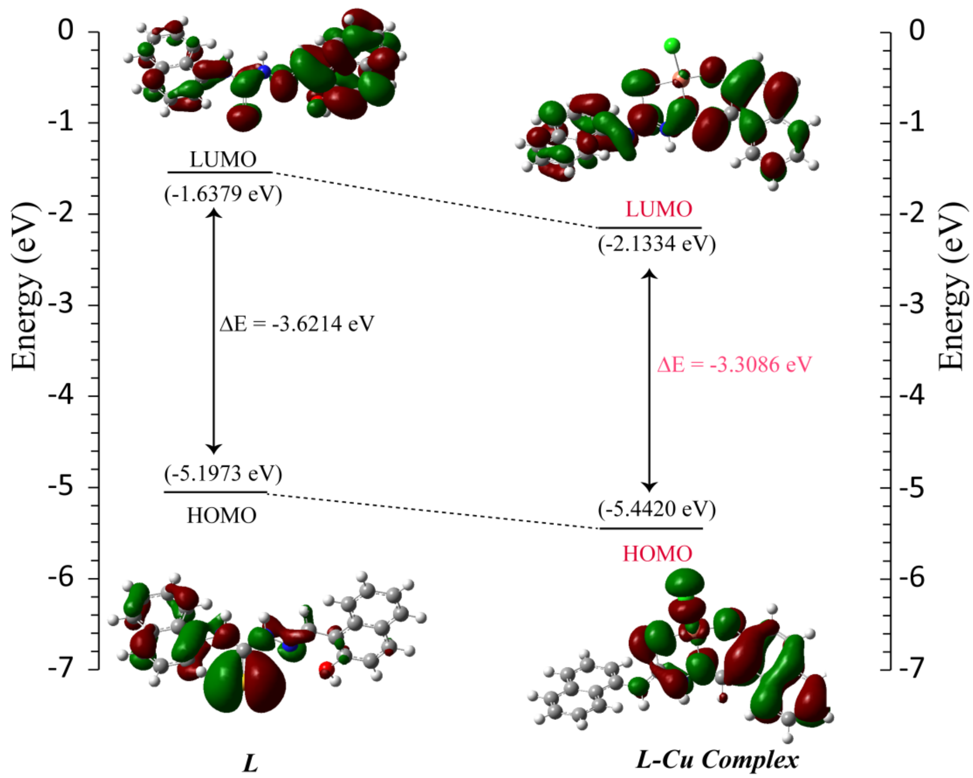

Figure S23: Frontier molecular orbital plots and energy level diagrams of **L** and **L**-Cu^{2+} complex. The calculations were performed using B3LYP/6-31 G (d,p) as implemented on Gaussian 03.

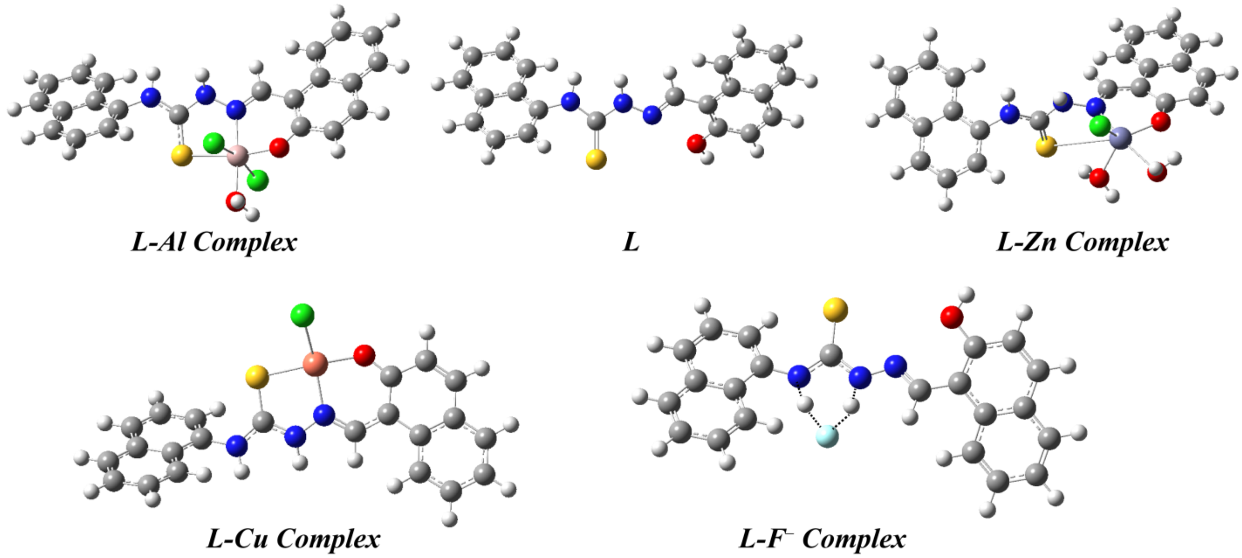

Figure S24: Optimized structures of L and its complexes. The calculations were performed using B3LYP/6-31 G (d,p) as implemented on Gaussian 03.

References:

1. M. J. Frisch, G. W. Trucks, H. B. Schlegel, G. E. Scuseria, M. A. Robb, J. R. Cheeseman, J. A. Montgomery, Jr., T. Vreven, K. N. Kudin, J. C. Burant, J. M. Millam, S. S. Iyengar, J. Tomasi, V. Barone, B. Mennucci, M. Cossi, G. Scalmani, N. Rega, G. A. Petersson, H. Nakatsuji, M. Hada, M. Ehara, K. Toyota, R. Fukuda, J. Hasegawa, M. Ishida, T. Nakajima, Y. Honda, O. Kitao, H. Nakai, M. Klene, X. Li, J. E. Knox, H. P. Hratchian, J. B. Cross, V. Bakken, C. Adamo, J. Jaramillo, R. Gomperts, R. E. Stratmann, O. Yazyev, A. J. Austin, R. Cammi, C. Pomelli, J. W. Ochterski, P. Y. Ayala, K. Morokuma, G. A. Voth, P. Salvador, J. J. Dannenberg, V. G. Zakrzewski, S. Dapprich, A. D. Daniels, M. C. Strain, O. Farkas, D. K. Malick, A. D. Rabuck, K. Raghavachari, J. B. Foresman, J. V. Ortiz, Q. Cui, A. G. Baboul, S. Clifford, J. Cioslowski, B. B. Stefanov, G. Liu, A. Liashenko, P. Piskorz, I. Komaromi, R. L. Martin, D. J. Fox, T. Keith, M. A. Al-Laham, C. Y. Peng, A. Nanayakkara, M. Challacombe, P. M. W. Gill, B. Johnson, W. Chen, M. W. Wong, C. Gonzalez, and J. A. Pople, *Gaussian 03, Revision E.01,Gaussian, Inc., Wallingford CT*, 2004.